Supporting Information for

An Instant Responsive Polymer Driven by Anisotropy of Crystal Phases

Heng Deng[#], Yuan Dong[#], Cheng Zhang, Yunchao Xie, Chi Zhang, and Jian Lin*

Department of Mechanical & Aerospace Engineering, University of Missouri,

Columbia, Missouri 65211, USA.

E-mail: LinJian@missouri.edu

# These authors contribute equally to this work

Supplementary Note: MD simulation

Construction of systems: All MD simulations were carried out by LAMMPS[1] which has been used by us to study a conversion of polymers to graphene under laser induced conditions[2] as well as to reveal the actuation mechanism of a programmable polymer gel.[3] Acetone and water molecules were modeled by the Pereyra, Asar, and Carignano (PAC) potential[4] and TIP5P-E potential,[5] respectively. These potentials enable to reproduce a full miscibility of acetone solution by accurately describing the change of the energy, entropy, and Helmholtz free energy of the mixtures.[6] Polymer crystals were simulated by the OPLS potential,[7] which ascribes the intermolecular energies including Van der Waals, and electrostatic energies, as well as intramolecular energies such as bonding energy, angle energy, and torsion energy. The OPLS potential gives the Lennard-Jones distance and energy parameters in each site of the organic molecules. The Lorentz−Berthelot rule was applied to these inter-site interactions. The long-range electrostatic interactions in the sites of the organic molecules were accounted by means of PPPM method.[8] The non-bonded repulsive interaction and real-space part of the Coulomb and dispersion terms were shifted at a truncated radius of 1 nm. Equilibrium structures of all the molecules were constructed and geometrically optimized in the Material Studio 7.0. The partial charge of each atom was calculated by the first-principle

calculation using VAMP package integrated in Material Studio 7.0. Then locations, bonds, and charges of each molecule were loaded into molecule template files, which were then used by Moltemplate package (http://www.moltemplate.org/) to build input files for LAMMPS. Periodic boundary conditions were implemented in all three Cartesian coordinate directions. Temperature and pressure were maintained using the Nose-Hoover barostats.

α- and β-PVDF crystals were built according to unit cell structures reported by literature[9, 10] (Figure S11).The unit cell of the α-PVDF crystal is orthorhombic with lattice constants of a = 4.96, b = 9.64, and c = 4.62 Å. The β-PVDF crystal also has an orthorhombic unit cell with lattice constants of a = 8.45, b = 4.88, and c = 2.55 Å. 20 polymer chains were built for both phases with each α-PVDF chain having 18 unit cells and each β-PVDF chain having 36 unit cells. As a result, there were the same number of total 216 atoms in each chain for both phases. [1 0 0] lattice planes of the α-PVDF crystal and [0 1 0] lattice planes of the β-PVDF crystal were exposed to aqueous acetone solution at various concentrations. By this way, the α-PVDF and β-PVDF crystals have similar dimensions. Thicknesses for the α crystal and the β crystal are 9.92 Å and 9.76 Å, respectively. Areas for them are 801.7 $Å^2$ and 775.7 $Å^2$, respectively.

The acetone-water mixtures have concentrations of acetone ranging from 20 wt% to 80 wt%. These mixtures were put in simulation boxes with the same x-y dimensions for each PVDF crystal. The z dimension was allowed to change as the systems were equilibrated under the NPT ensemble. The equilibration was carried out at T = 300 K and P_z = 1 atm for 1 ns. Then the mixtures were contacted with the PVDF crystals in the simulation boxes. The initial distance between the mixtures and PVDF was set to be 5 Å, which was changed to desired distances after the systems were relaxed. During the simulation, the mixed systems were kept under the NPT ensembles for 10 ns. Then intermolecular energies between PVDF and solute species were calculated to compare the affinity of acetone to α-PVDF and β-PVDF

crystals. Spatial distribution of acetone and water around PVDF crystals were analyzed by calculating their number densities in z directions (z). Mean squared displacement (MSD) of acetone molecules at a distance of < 2.5 Å to the surfaces of PVDF crystals were calculated to estimate the diffusivity of the acetone.

Results and explanations for simulation

The intermolecular energies caused by interactions of the α- and β-PVDF crystals with acetone (E_{PA}) and water (E_{PW}) in aqueous acetone solution were calculated. Representative ρ(z) for acetone:water mixtures with acetone concentration of 40 wt% are presented in Figure 3c. It shows that the acetone concentration on the surface of α-phase PVDF crystal is higher than that on the β-PVDF crystal. In opposite, the water concentration is lower. Excess adsorption coefficients[11, 12] of acetone and water on α-phase crystal over those of the β-phase crystal are defined as

$$\Gamma_{A(\alpha-\beta)} = \int_0^{z_0} \left[\rho_{A\alpha}(z) - \rho_{A\beta}(z) \right] \mathrm{dz} \quad \text{(Eq. 1)}$$

$$\Gamma_{W(\alpha-\beta)} = \int_0^{z_0} \left[\rho_{W\alpha}(z) - \rho_{W\beta}(z) \right] \mathrm{dz} \quad \text{(Eq. 2)}$$

where z_0 = 0.75 nm. Since the crystals occupy the space from z=-0.5 nm to z=0.5 nm, the integrals in Eqs. (1) and (2) depict the integrated amount of solvent in the region within distances of 2.5 Å to the crystal surfaces. The subscripts A indicates the acetone, and W indicates the water, α and β indicate the α- and β- phases. Table S1 lists $\Gamma_{A(\alpha-\beta)}$ and $\Gamma_{W(\alpha-\beta)}$ for solution with different acetone concentrations. The results indicate that the acetone is closer to the α-phase crystal than β-phase crystal. It indicates that the adsorption ability of the α-PVDF crystal toward acetone is stronger than that of the β-PVDF crystal.

The time evolution of MSD is shown in Figure 3d for the systems constructed with pure acetone. The diffusivity on surface can be calculated by the Einstein relation:[13]

$$D = \frac{1}{6t} \langle |R(t) - R(0)|^2 \rangle \quad \text{(Eq. 3)}$$

where R is the distance of random walk of molecules, t is the simulation time. The function $\langle |R(t) - R(0)|^2 \rangle$ is the MSD, which is a measure of the deviation over time between the position of a particle and its reference position. MSD can be directly calculated from the function integrated in LAMMPS. Here only the displacement in x and y directions (in-plane directions) were accounted to reflect the surface diffusion of acetone.

Supplementary Figures & Caption

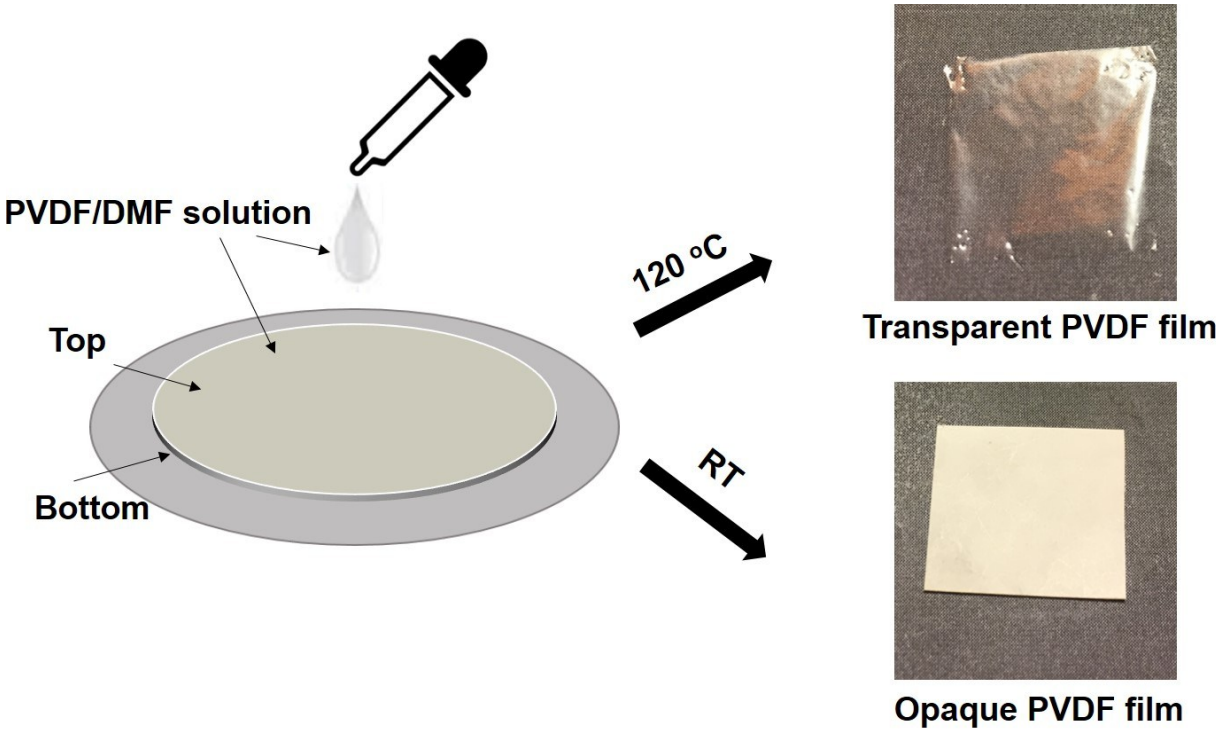

Figure S1. Scheme of fabrication processes for PVDF films. The transparent PVDF film and opaque PVDF film were obtained at different drying temperatures.

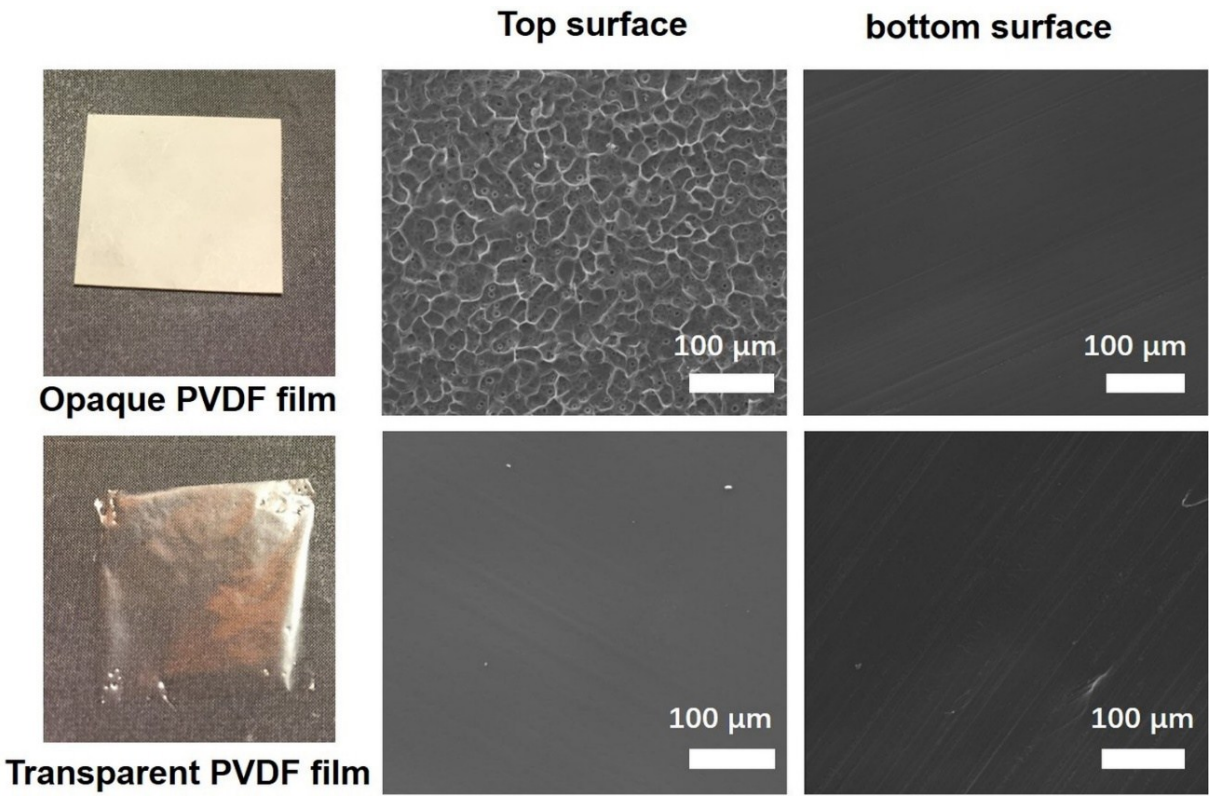

Figure S2. SEM images of opaque PVDF and transparent PVDF films. In the transparent PVDF film, both the top and bottom surfaces exhibit the same smooth morphology. However, in the opaque PVDF film, the top surface is porous and rough while the bottom surface is smooth. It should be noted that the porous architecture itself doesn't cause the response of the polymer film to stimuli, but accelerate the actuation speed by providing quick access of the stimuli to the pores of the film.[12] This explains why even though opaque PVDF possessed the porous structure (Figure S3) it doesn't respond to the acetone vapor (Figure S6).

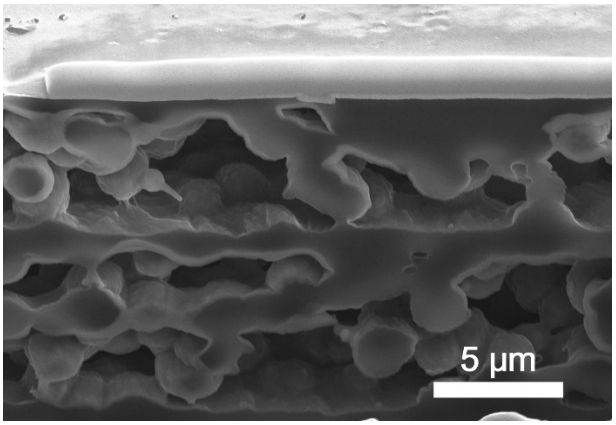

Figure S3. Cross-sectional SEM image of opaque PVDF film showing its porous structure.

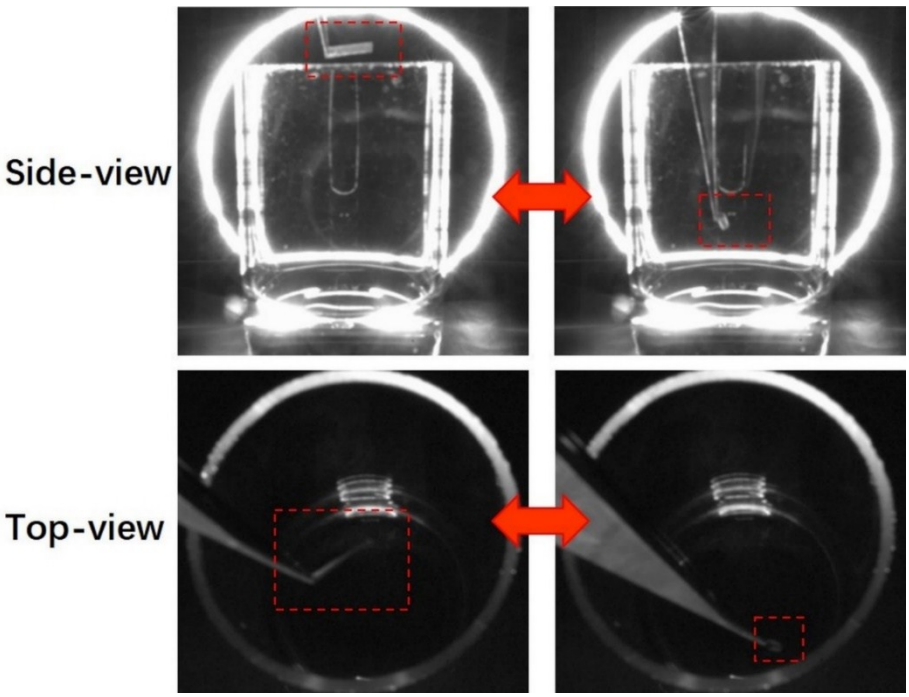

Figure S4. Optical images of responsive transparent PVDF films without dyes. These images show that the response of the transparent PVDF films is not a result of the dyes.

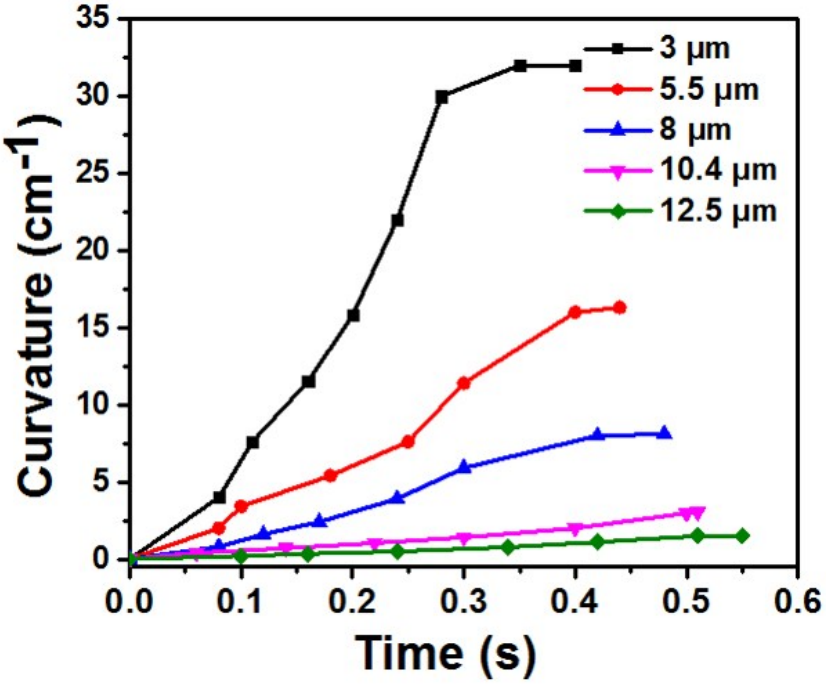

Figure S5. Plot of curvatures versus time for the transparent PVDF strips with different thickness varying from 3 µm to 12,5 µm. The PVDF films were made by controlling the spinning speed (1000 rpm to 3000 rpm) of the coater. All these films show fast response to acetone vapor (0.4 s to 0.6 s). The maximum bending curvatures of the PVDF films decrease as the thickness increases. This could be explained by a previous study which suggested the curvature of bending scales is inversely proportion to the film thickness.[14]

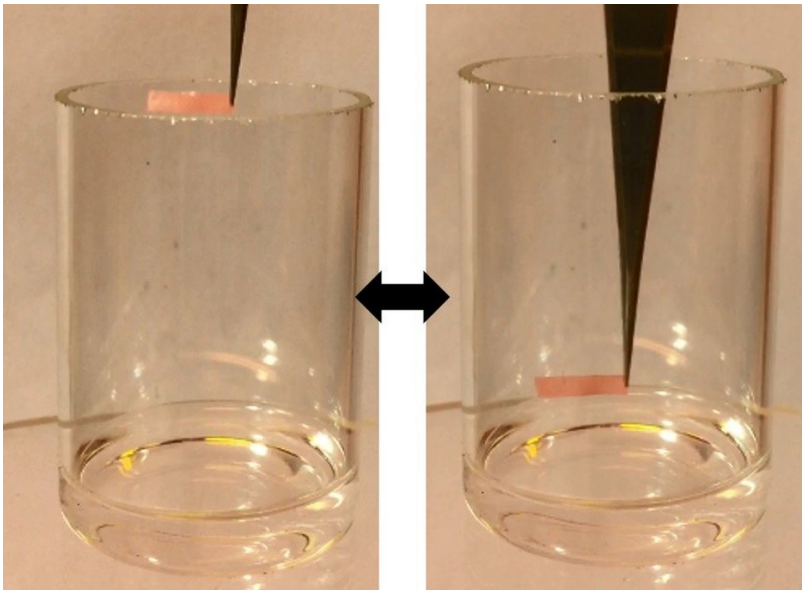

Figure S6. Optical images of an opaque PVDF film in acetone vapor. It shows no response in the acetone vapor.

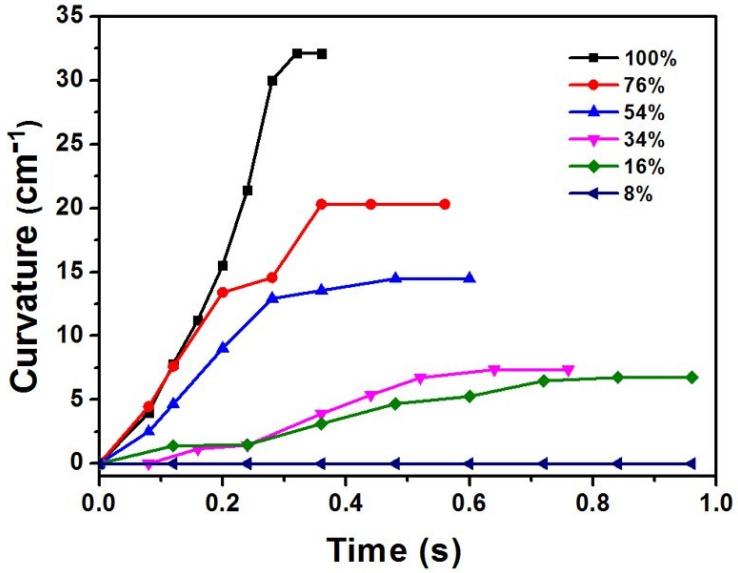

Figure S7. Curvatures of transparent PVDF strips responding to the vapor evaporating from acetone solution with different weight concentrations (wt%). Partial vapor pressure of acetone was calculated by Raoult's law ($P_A = P_A^*.X_A$),[15] where P_A^* is the vapor pressure of the pure acetone, and X_A is the mole fraction of acetone in the solution. For instance, a partial vapor pressure of acetone in 16 wt% solution was calculated to be 1.71 kPa (P_A^* = 30 kPa, X_A = 0.057, P_A=1.71 kPa).

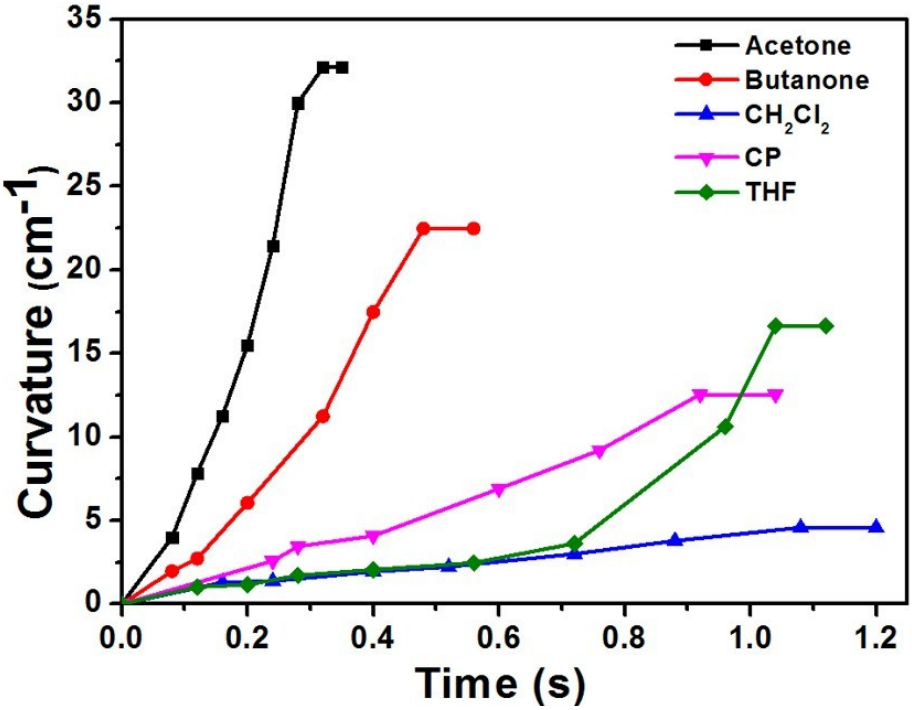

Figure S8. Curvatures of transparent PVDF strips responding to different organic vapors. Besides these solvents, ethanol, methanol, toluene, and isopropyl amine were also tested, but they do not actuate the transparent PVDF strips.

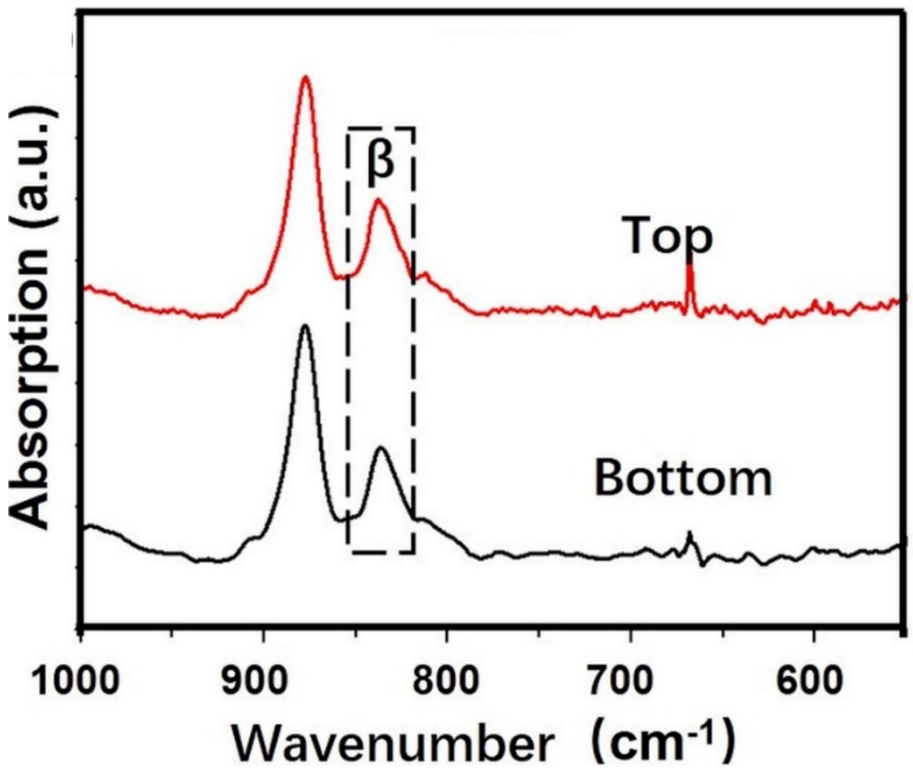

Figure S9. FTIR spectra of the top side and bottom side of an opaque PVDF film.

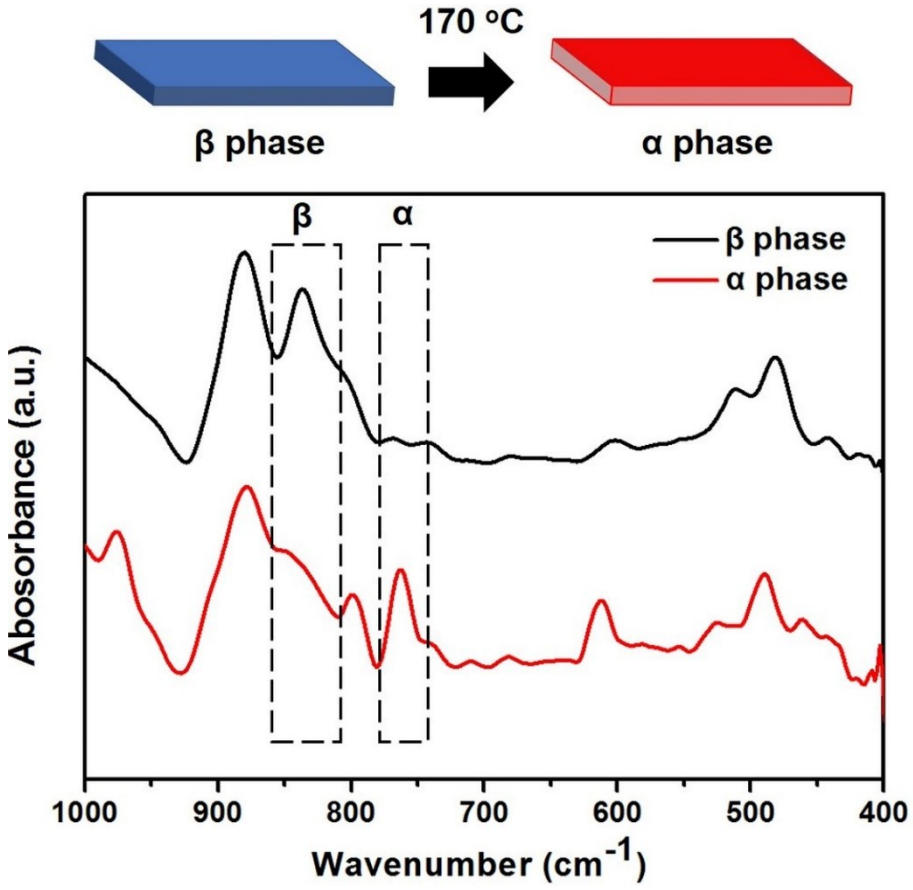

Figure S10. A scheme of transferring a homogeneous β-PVDF film into a homogeneous α-PVDF film (top panel) and their corresponding FTIR spectra (bottom panel).

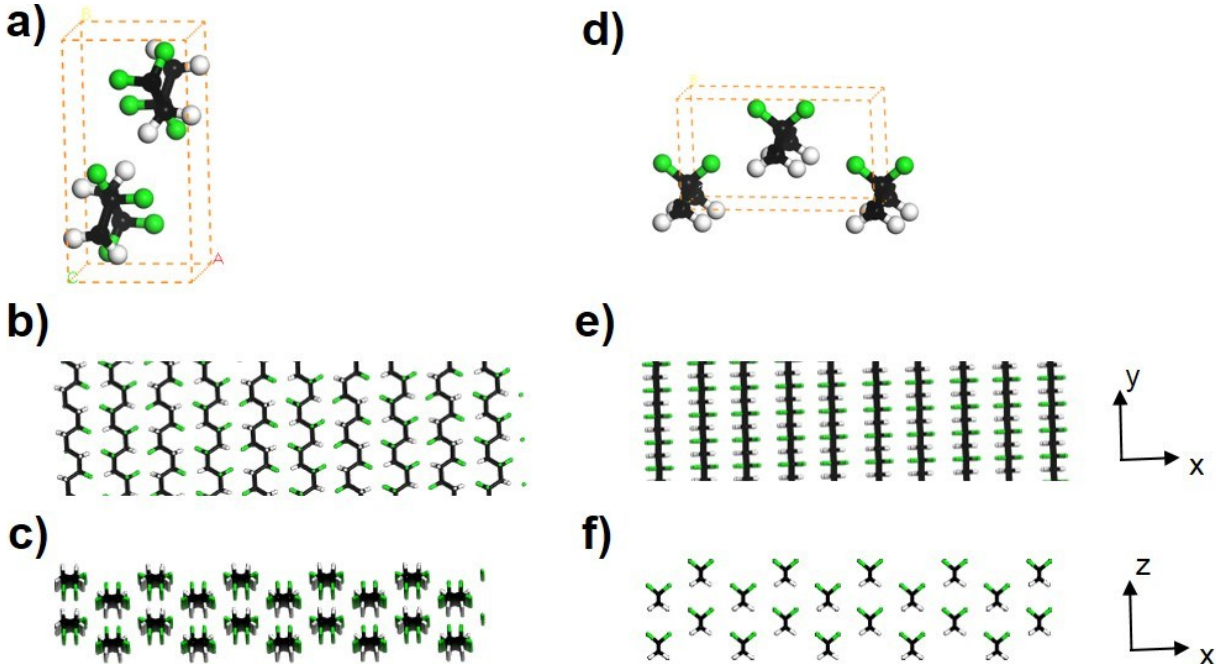

Figure S11. System construction for MD simulation. **(a)** Unit cell, **(b)** Top view, **(c)** and front view of α-PVDF crystals. (d) Unit cell, (e) Top view, (f) and front view of β-PVDF crystals.

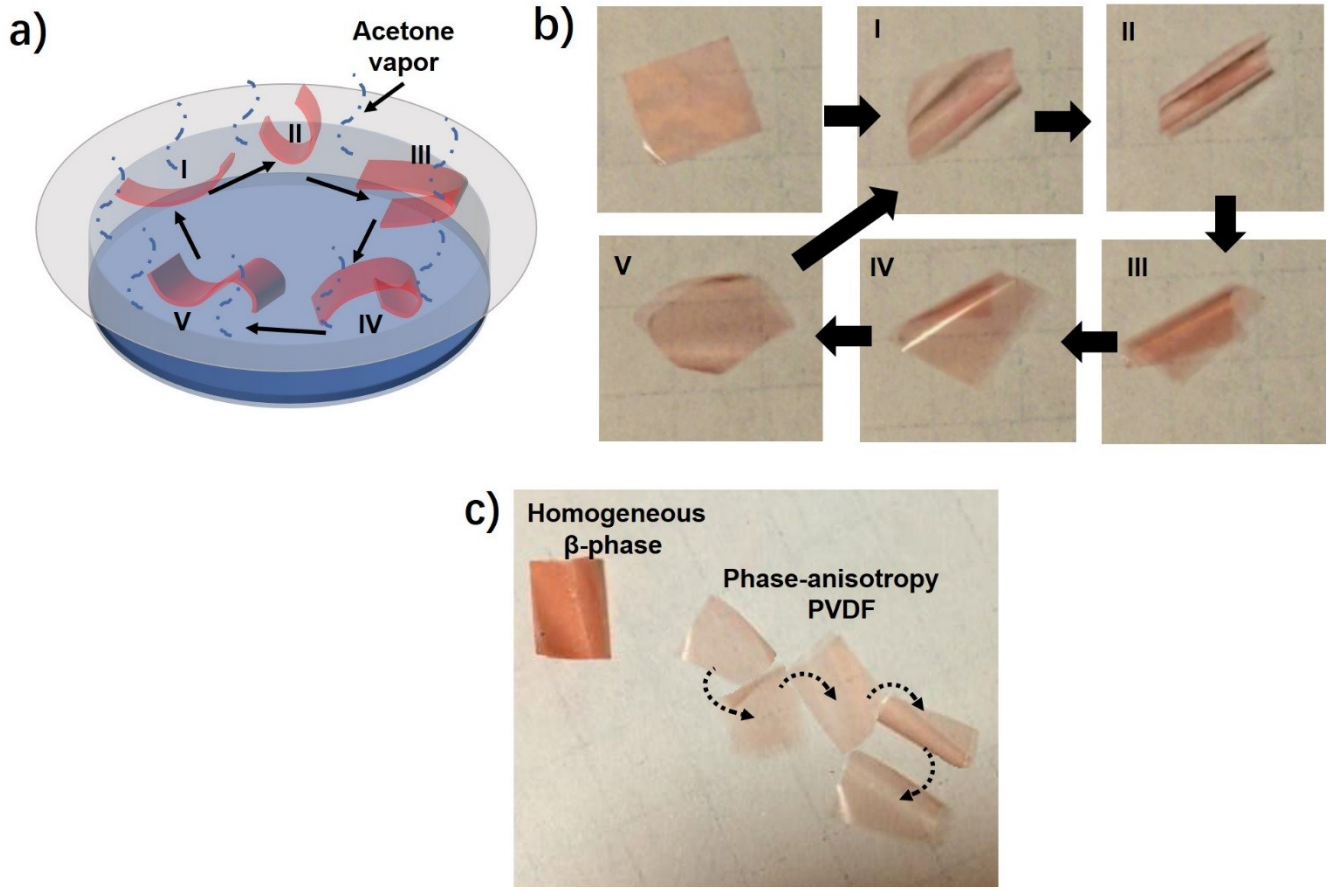

Figure S12. (a) Scheme of a phase-anisotropy PVDF film without Ni particles showing autonomous locomotion on a porous paper substrate covering the acetone solution. Due to vapor evaporation, a gradient of acetone vapor was generated in the evaporation pathway. **(b)** Mechanism of locomotion of the phase-anisotropy PVDF film (5 mm x 5 mm). **(c)** Optical image showing the distinct locomotion behaviors of a phase-anisotropy PVDF and a homogeneous β-PVDF film in the acetone vapor.

The fabricated phase-anisotropy PVDF film without Ni particles can be flipped over by acetone with a concentration gradient, which results in continuous locomotion on the paper. A typical locomotive cycle of the phase-anisotropy PVDF film is composed of the following five stages (Figure S12a-b, Movie S4). When a phase-anisotropy PVDF film is put on the porous paper substrate, the face closed to vapor source absorbs more acetone than the other one, causing asymmetric swelling that make the film curves up (I).

As the film curves further, the film's gravity center rises, and the film becomes mechanically unstable (II) and eventually the curved film slips over to the other side (III). A quick acetone desorption of the curved edge parts, lead to horizontal movement (IV). Finally, the curved edge parts of the film fall back to the substrate with original top surface contacting substrate, resulting a new asymmetric acetone swelling (V) to restart the cycle (I). By contrast, the homogeneous β-PVDF strip only stays static on the paper (Figure S12c), which further indicates the different responses of the homogeneous β-PVDF and phase-anisotropy PVDF films to the acetone vapor.

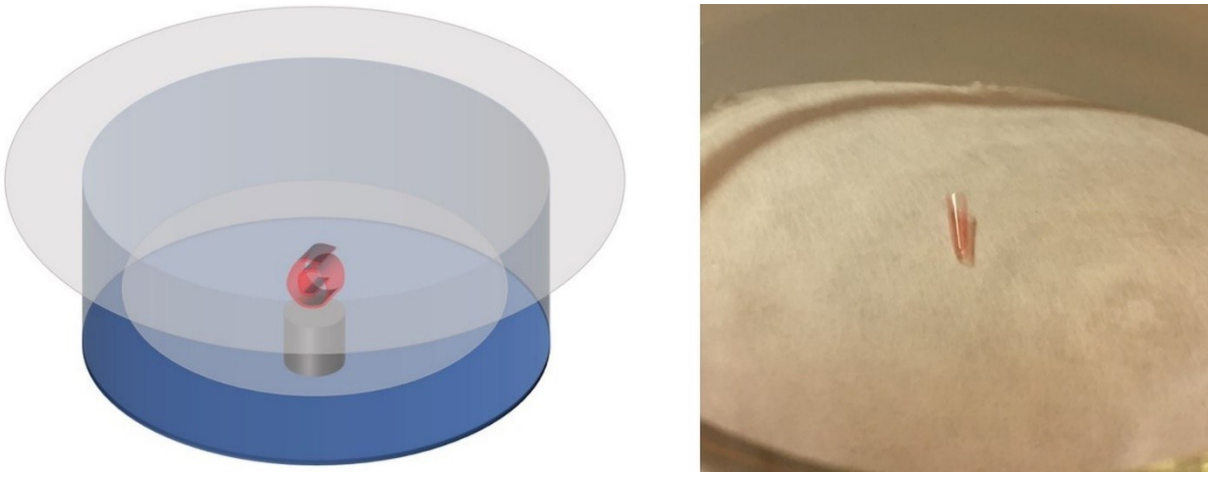

Figure S13. A scheme and an optical image of a phase-anisotropy PVDF film folding into a roll and remains static in homogenous acetone vapor.

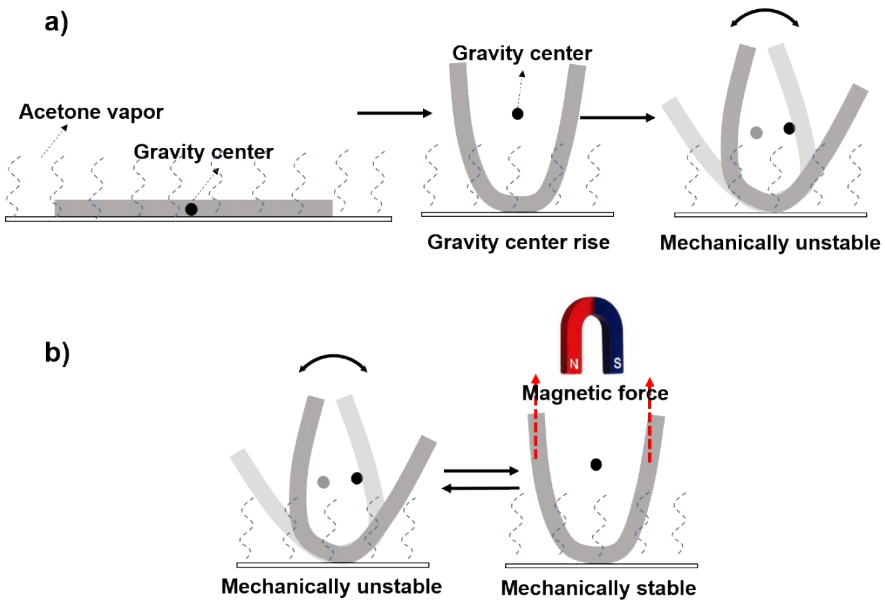

Figure S14. Scheme of the mechanism of the magnetically controlled soft tumbler. (**a**) When the film is curved due to the absorption of acetone vapor, its gravity center rises, making it mechanically unstable. And the increased weight from the added Ni particles make the acetone vapor powerless to slip the film over to the other side. As a result, the curved film wiggles from one side to the other in the acetone vapor with a concentration gradient. (**b**) Due to the magnetic force, the curved film will become mechanically stable. And when the magnetic field is moved, it will become mechanically unstable again. Therefore the magnet served as a remote switch to control the movement of the soft tumbler.

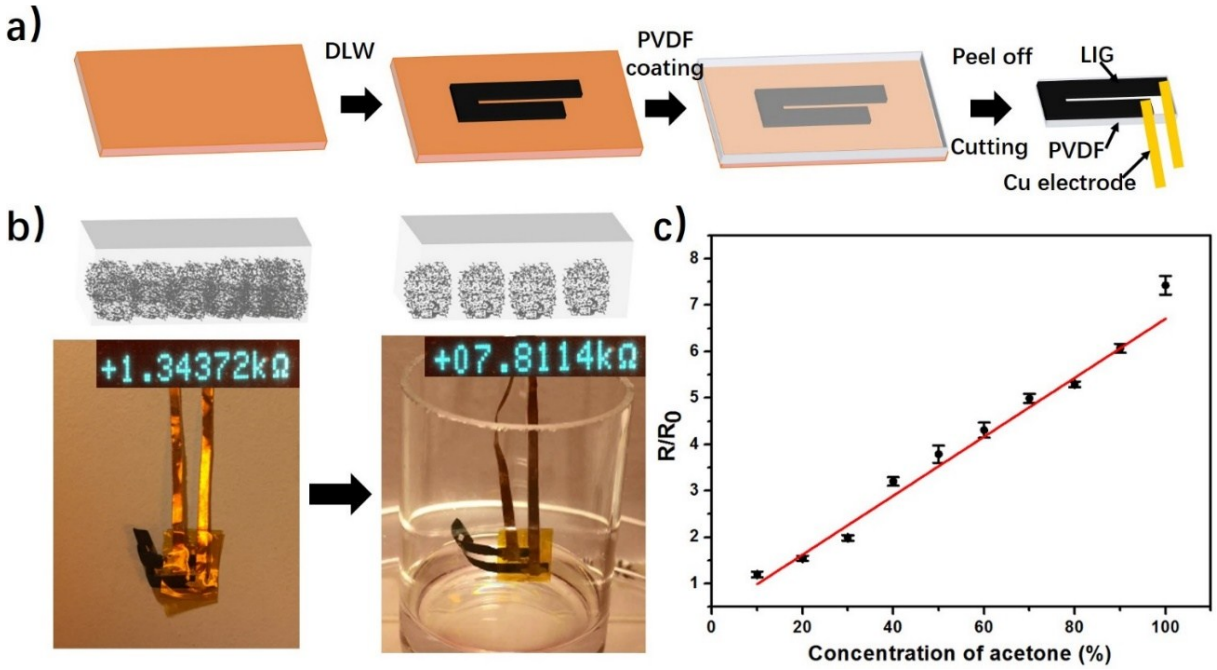

Figure S15. (a) A scheme of fabrication process for a LIG-PVDF chemi-mechanical sensor. **(b)** Schemes showing the change of distance of conductive network when the device responds to acetone vapor. Optical images showing change of resistance of a LIG-PVDF sensor when responding to acetone vapor. **(c)** Relative resistance change of a LIG-PVDF sensor at aqueous acetone solution with various concentrations.

Here, we demonstrate that electronic elements can be imbedded into the PVDF matrix to make a chemi-mechanical sensor. In this study, we combined the phase-anisotropy PVDF with conductive laser-induced graphene (LIG) (Figure S15a). The porous structure of the LIG is well suited for infiltration of the PVDF solution. Thanks to the effective infiltration of PVDF solution, the LIG film can be successfully peeled of the polyimide substrate. Due to the strain mismatch between LIG layer and PVDF layer, the peeled LIG-PVDF film is naturally curved from LIG side to the PVDF side (Figure S15b). When this curved LIG-PVDF film was exposed to the acetone vapor, it became flat (Figure S15b), causing a remarkable increase of the resistance of the device (Figure S15b). While the device was put back to air,

its resistance was recovered to a lower value. The basic mechanism of the resistance change in LIG/polymer based strain sensor has been reported.[16] The applied strain increases the spacing of the conductive network in the LIG, thus lowering the number of contact points and resulting in an increase of the electrical resistance. This spacing recovers to the original state when the device is exposed to air. Unlike the previous report,[16] in which artificial strain needed to be applied to change the spacing of the conductive network, the increase of spacing of the conductive network in the LIG was a result of the responsive swelling of the PVDF. Because the swelling volume of the PVDF depends on the concentration of the acetone vapor (Figure S15c), the fabricated LIG-PVDF sensor exhibited linear change of the resistance versus concentration, indicating the potential of using LIG-PVDF as a chemi-mechanical sensor.

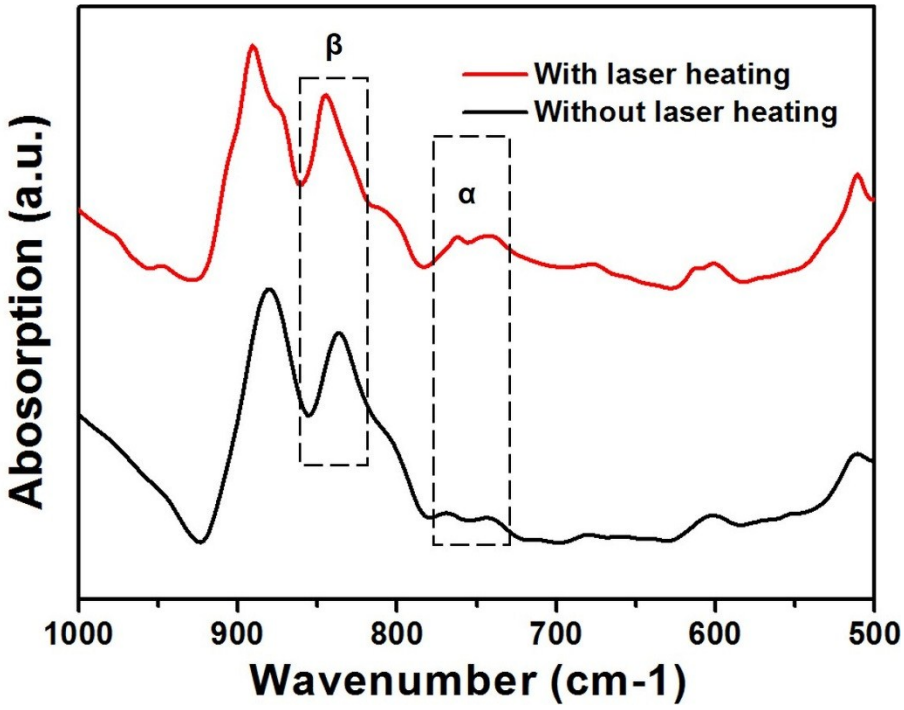

Figure S16. FTIR spectra of homogeneous β-PVDF films taken from the areas with or without laser irradiation.

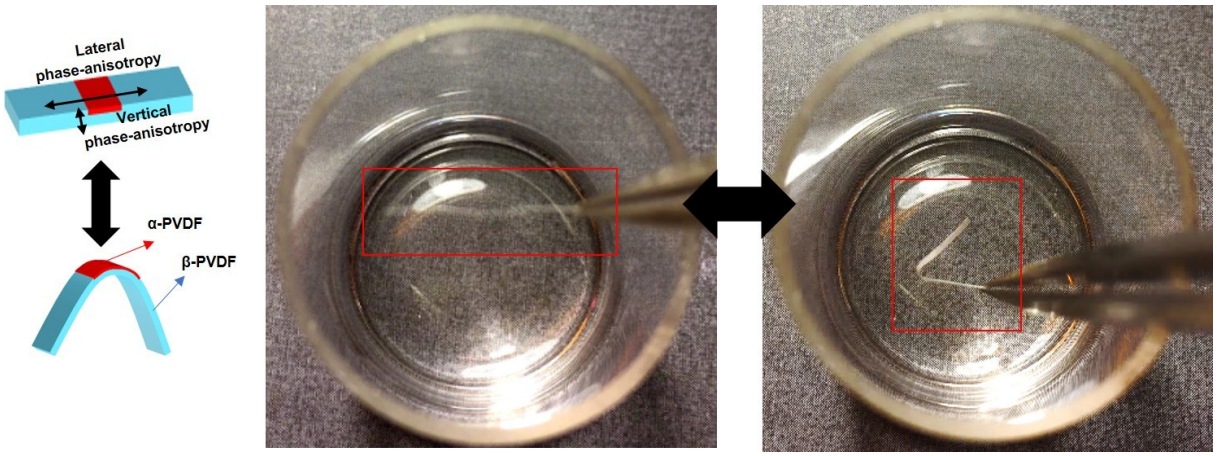

Figure S17. Scheme and optical images showing localized folding of a laser-irradiated homogeneous β-PVDF strip.

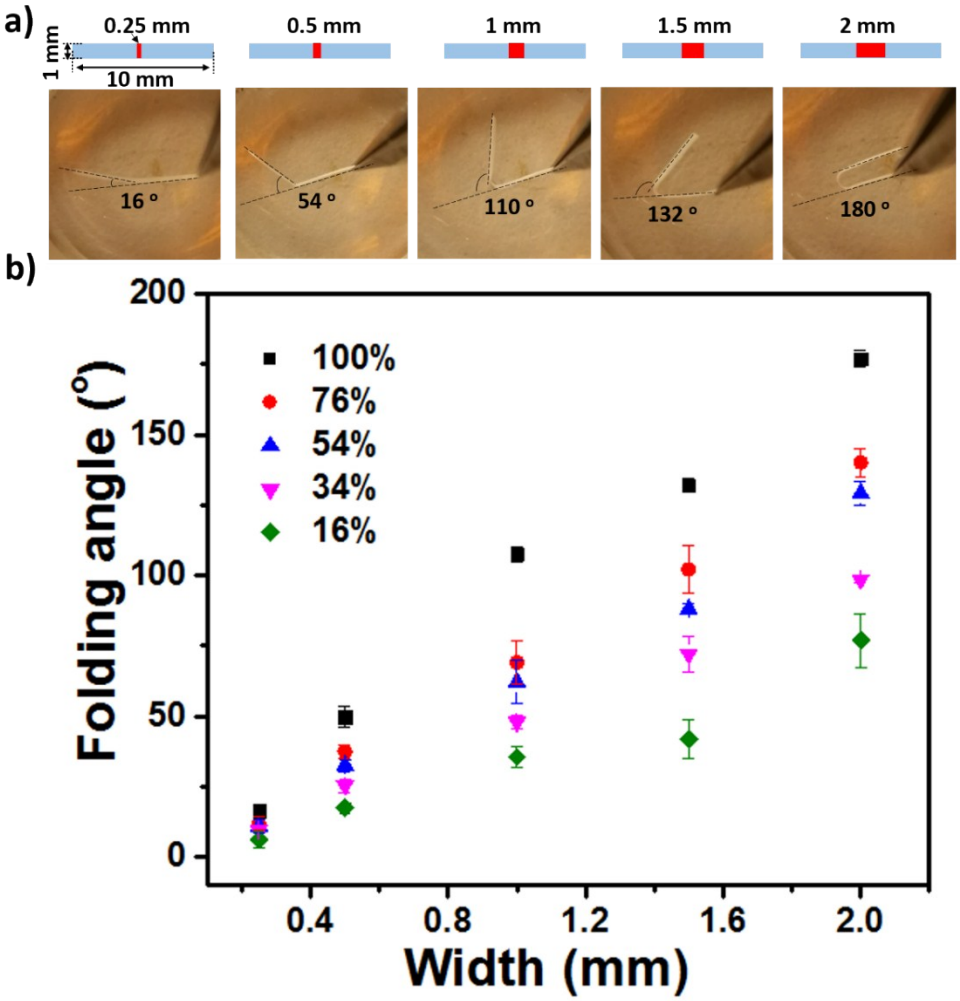

Figure S18. (**a**) Optical images showing the folding angles of PVDF strips (1 mm x 10 mm) with different crease width to 100 wt% acetone. The active crease (red) with different widths (0.25 mm, 0.5 mm, 1 mm, 1.5 mm, and 2.0 mm) were laser patterned at the middle of these PVDF stripes (1 mm x 10 mm). (**b**) Plots of the folding angles of the PVDF strips with different crease widths at aqueous acetone solution with different weight concentrations. These results suggested the width of crease and acetone concentration has a big influence on the bending behaviors. As the width of crease increases, the folding angle of the PVDF stripes increases, which is in good agreement with previous studies.[3, 17] As the acetone concentration decreases, the folding angel of the PVDF stripes decreases, which is in agreement with our previous observation (Figure S7).

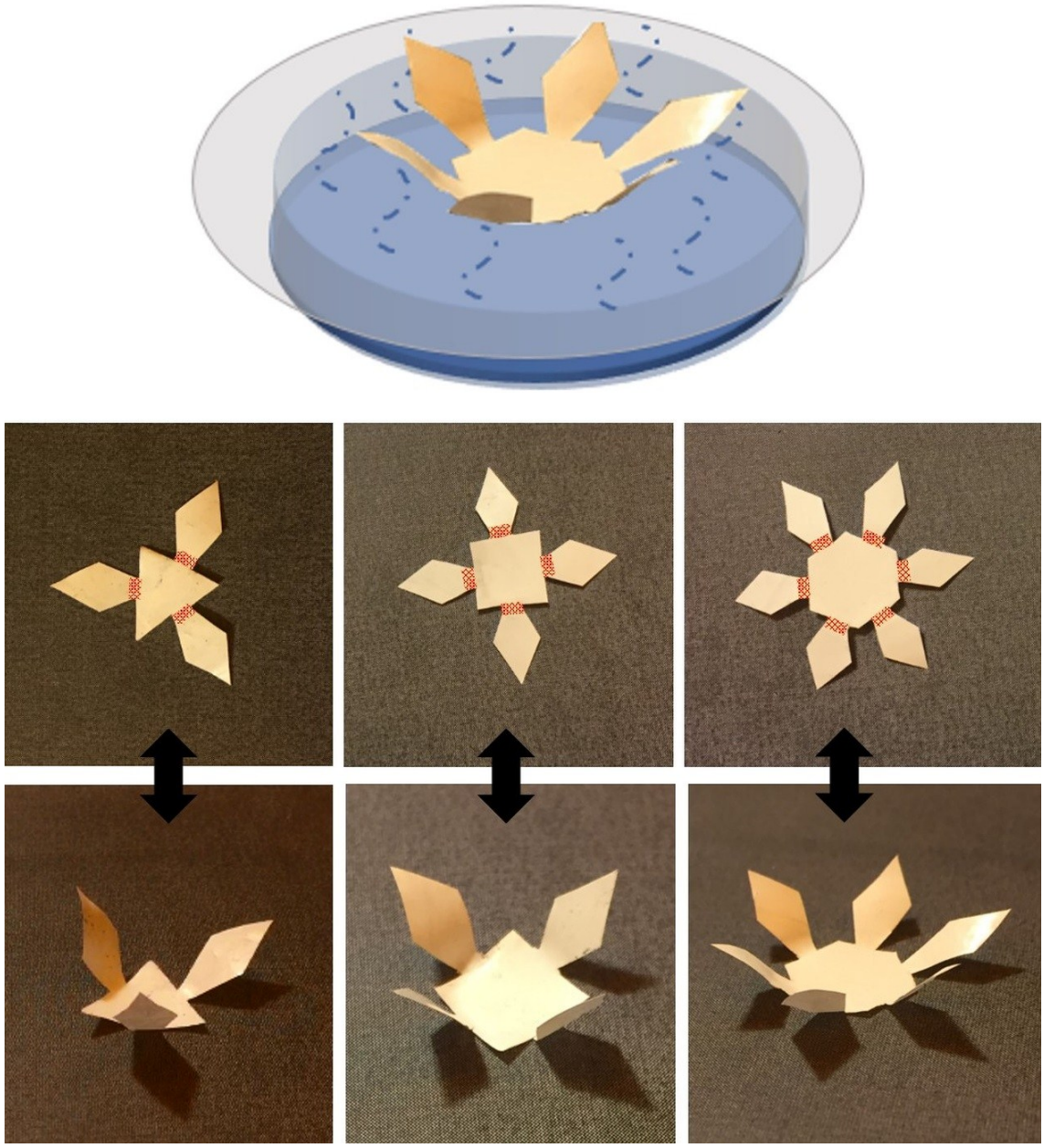

Figure S19. Scheme and optical images of a laser-irradiated origami PVDF film evolved into 3D structures on a porous paper substrate covering acetone solution. A gradient of the acetone concentration is generated due to acetone evaporation from the solution.

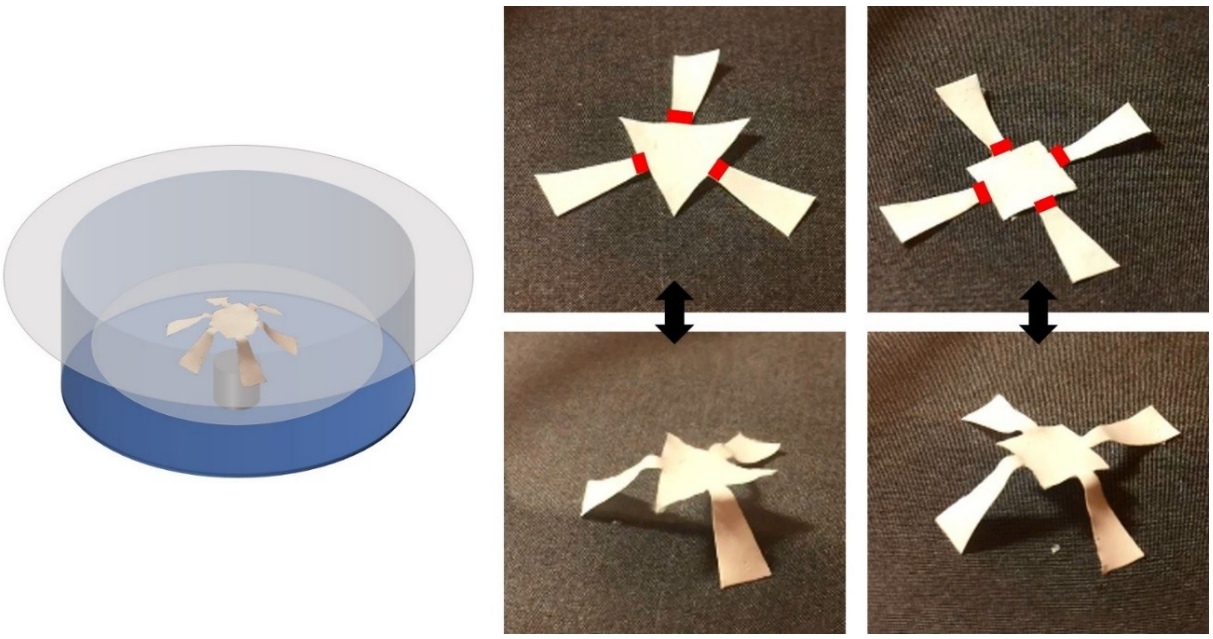

Figure S20. Scheme and optical images of a laser-irradiated origami PVDF film evolved into 3D structures in the homogenous acetone vapor.

Supplementary Tables

Table S1. Excess adsorption coefficients of α-phase and β-phase PVDF crystals toward acetone and water.

wt% acetone	$\Gamma_{A(\alpha-\beta)}$	$\Gamma_{W(\alpha-\beta)}$
20	+0.0031	-0.0071
40	+0.0026	-0.0063
60	+0.0016	-0.0009
80	+0.0020	+0.0009

Supplementary References

1. S. Plimpton, *J. Comput. Phys.*, 1995, **117**, 1-19.
2. Y. Dong, S. C. Rismiller and J. Lin, *Carbon*, 2016, **104**, 47-55.
3. H. Deng, Y. Dong, J.-W. Su, C. Zhang, Y. Xie, C. Zhang, M. R. Maschmann, Y. Lin and J. Lin, *ACS Appl. Mater. Inter.*, 2017, **9**, 30900-30908.
4. R. G. Pereyra, M. L. Asar and M. A. Carignano, *Chem. Phys. Lett.*, 2011, **507**, 240-243.
5. S. W. Rick, *J. Chem. Phys.*, 2004, **120**, 6085-6093.
6. A. Pinke and P. l. Jedlovszky, *J. Phys. Chem. B* 2012, **116**, 5977-5984.
7. W. L. Jorgensen, D. S. Maxwell and J. Tirado-Rives, *J. Am. Chem. Soc.*, 1996, **118**, 11225-11236.
8. B. A. Luty and W. F. van Gunsteren, *J. Phys. Chem.*, 1996, **100**, 2581-2587.
9. R. Hasegawa, M. Kobayashi and H. Tadokoro, *Polym. J.*, 1972, **3**, 591-599.
10. R. Hasegawa, Y. Takahashi, Y. Chatani and H. Tadokoro, *Polym. J.*, 1972, **3**, 600-610.
11. V. Pierce, M. Kang, M. Aburi, S. Weerasinghe and P. E. Smith, *Cell Biochem. Biophys.*, 2008, **50**, 1-22.
12. Q. Zhao, J. W. Dunlop, X. Qiu, F. Huang, Z. Zhang, J. Heyda, J. Dzubiella, M. Antonietti and J. Yuan, *Nat. Commun.*, 2014, **5**, 4293.
13. W. Fang, L. Zhang and J. Jiang, *J. Phys. Chem. C*, 2011, **115**, 14123-14130.
14. S. Timoshenko, *JOSA*, 1925, **11**, 233-255.
15. F. Raoult, *Comptes Rendus*, 1887, **104**, 1430-1433.
16. R. Rahimi, M. Ochoa, W. Yu and B. Ziaie, *ACS Appl. Mater. Inter.*, 2015, **7**, 4463-4470.
17. J. H. Na, A. A. Evans, J. Bae, M. C. Chiappelli, C. D. Santangelo, R. J. Lang, T. C. Hull and R. C. Hayward, *Adv. Mater*., 2015, **27**, 79–85